Hindawi
Molecular Imaging
Volume 2023, Article ID 4200142, 11 pages
https://doi.org/10.1155/2023/4200142

Research Article

Development and Evaluation of a Novel Radiotracer ^{125}I-rIL-27 to Monitor Allotransplant Rejection by Specifically Targeting IL-27Rα

Shanshan Zhao,[1,2] **Qian Liu**,[3] **Feng Gao**,[2] **and Guihua Hou**[2]

[1]*Department of Pathology, The Second Affiliated Hospital of Zhejiang University School of Medicine, Hangzhou, Zhejiang 310009, China*
[2]*Key Laboratory for Experimental Teratology of the Ministry of Education and Biomedical Isotope Research Center, School of Basic Medical Sciences, Cheeloo College of Medicine, Shandong University, Jinan, Shandong 250012, China*
[3]*Department of Radiology, The Second Affiliated Hospital of Zhejiang University School of Medicine, Hangzhou, Zhejiang 310009, China*

Correspondence should be addressed to Guihua Hou; ghhou@sdu.edu.cn

Received 2 October 2022; Revised 9 January 2023; Accepted 2 February 2023; Published 23 February 2023

Academic Editor: Henry VanBrocklin

Noninvasive monitoring of allograft rejection is beneficial for the prognosis of patients with organ transplantation. Recently, IL-27/IL-27Rα was proved in close relation with inflammatory diseases, and ^{125}I-anti-IL-27Rα mAb our group developed demonstrated high accumulation in the rejection of the allograft. However, antibody imaging has limitations in the imaging background due to its large molecular weight. Therefore, we developed a novel radiotracer (iodine-125-labeled recombinant IL-27) to evaluate the advantage in the targeting and imaging of allograft rejection. In vitro specific binding of ^{125}I-rIL-27 was determined by saturation and competitive assay. Blood clearance, biodistribution, phosphor autoradioimaging, and IL-27Rα expression were studied on day 10 after transplantation (top period of allorejection). Our results indicated that ^{125}I-rIL-27 could bind with IL-27Rα specifically and selectively in vitro. The blood clearance assay demonstrated fast blood clearance with 13.20 μl/h of ^{125}I-rIL-27 staying in the blood after 24 h. The whole-body phosphor autoradiography and biodistribution assay indicated a higher specific uptake of ^{125}I-rIL-27 and a clear radioimage in allograft than in syngraft at 24 h, while a similar result was obtained at 48 h in the group of ^{125}I-anti-IL-27Rα mAb injection. Meanwhile, a higher expression of IL-27Rα was found in the allograft by Western blot. The accumulation of radioactivity of ^{125}I-rIL-27 was highly correlated with the expression of IL-27Rα in the allograft. In conclusion, ^{125}I-rIL-27 could be a promising probe for acutely monitoring allograft rejection with high specific binding towards IL-27Rα on allograft and low imaging background.

1. Introduction

Solid organ allotransplantation has been the most effective therapeutic strategy for patients with end-stage organ failure [1, 2]. However, the appearance of acute rejection is strongly related to the loss of allograft and a poor prognosis [3]. Therefore, early detection of acute rejection with the noninvasive method could greatly improve the prognosis after organ transplantation [4].

Recently, IL-27Rα (interleukin-27 receptor α), along with its ligand (IL-27), has been shown to trigger the immune response, including cancer, abdominal aortic aneurysm, Sjögren syndrome, virus infection, and transplantation [5–9]. IL-27Rα is the specific subunit of the IL-27 receptor and is restricted primarily to lymphocytes and monocytes [10]. The IL-27 pathway has been shown to inhibit tumor growth by enhancing the response of T cells and decreasing the proportion of Treg cells (T regulator cells) [11]. Furthermore, IL-27

showed a proinflammatory effect by enhancing the IL-1β (interleukin-1 β) secretion from monocytes and macrophages [12]. Moreover, IL-27 could also promote the function of NK cells (natural killer cells) by secreting more IFN-γ (interferon-γ) during influenza infection [13]. All of this suggested that IL-27 could activate IL-27Rα and enhance the proinflammation response.

Acute rejection of the allograft was a severe proinflammatory response participated by T cells and macrophages, and IL-27 has been shown to be closely related to allograft rejection [8, 14, 15]. IL-27Rα (IL-27 receptor α) expression in T cells exacerbated GVHD (graft-versus-host disease) by improving the effector function of Th1 cells (T helper 1 cells) and inhibiting subsets of Th2 and Treg cells [8], while IL-27Rα was apparently upregulated in alloreactive splenetic $CD4^+$T cells, T cells, and macrophage when acute rejection occurred [16–18]. In our previous study with the allografted mouse model, we found that a large amount of IL-27Rα-positive T cells and macrophage infiltrated in the rejection of the allograft and anti-IL-27Rα mAb labeled with iodine-125 could obviously accumulate in the allograft noninvasively when rejection occurred [19].

Target tissue could be accurately and noninvasively diagnosed by molecular nuclear imaging with a specific probe, which was much more favorable than histopathological biopsies and traditional imaging examination [20–24]. Although histopathological biopsies were the "gold standard" of acute graft rejection, they still were an invasive examination and can induce complications, including pain, bleeding, and death [25, 26]. Noninvasive examinations, such as magnetic resonance imaging and ultrasound, reflected decreased graft function and were limited in targeting allograft [22, 24]. Targeted molecular imaging has advantages in tracking specific cells and monitoring the function of the target organ with probes that have detection signals [27–29]. Among them, radionuclide imaging was a noninvasive method by which a disease could be diagnosed effectively and quickly, and the therapeutic effect could be monitored with the help of a radio probe. Radionuclide imaging with radiolabeled macromolecular objects such as proteins and antibodies usually had the disadvantages of long time to reach the target tissue and the high background, resulting in poor image quality. However, small molecules could quickly accumulate in the target tissue and thus improve imaging. Therefore, the small-sized radio probe is a much more promising radiotracer in radionuclide imaging than the full-length antibody. Radiolabeled cytokines have been applied to track targeted immunocytes due to high contrast imaging, fast clearance, low background, and weak inflammation response [30–32]. Hartimath et al. developed [^{18}F] FB-IL-2 to monitor activated T lymphocyte infiltration induced by cancer therapy in tumor [33]. Di Gialleonardo et al. demonstrated that ^{18}F-FB-IL-2 could trace IL-2 receptor-positive cells [34]. [^{124}I] I-F8-IL-10 could accumulate in a patient with arthritic joints in rheumatoid arthritis. Meanwhile, fast clearance of [^{124}I] I-F8-IL10 and [^{131}I] I-F8-IL-10 in nonspecific target tissues was found in a 24-hour span [35]. Consequently, imaging with radiolabeled cytokines had the advantage of specific recognition of target tissue with a low background and could be a promising strategy for allorejection detection.

In this study, we prepared a novel radio probe (^{125}I-labeled recombinant IL-27, ^{125}I-rIL-27) to specifically target IL-27Rα and evaluated its potential application in monitoring acute allograft rejection.

2. Materials and Methods

2.1. Chemicals, Reagents, and Equipment. IL-27Rα mAb was obtained from the R&D system (Minnesota, USA). Recombination IL-27 (rIL-27) was purchased from PeproTech (New Jersey, USA). Na^{125}I was provided by the China Institute of Atomic Energy (Beijing, China). The Sephadex G-25M PD10 column was purchased from GE Healthcare (Pennsylvania, USA). RPMI-1640 medium was obtained from Biological Industries (Kibbutz Beit Haemek, Israel). Bromophenol orchid, HEPES buffer, BSA (bovine albumin) and red blood cell lysis buffer were obtained from Solarbio (China, Beijing). SDS (sodium dodecyl sulfate) loading buffer, antibody dilution buffer, and blocking buffer were obtained from Beyotime (Shanghai, China). PBS (phosphate-buffered saline), TBST (tris-buffered saline and Tween) buffer, H&E (hematoxylin and eosin) staining, and immunofluorescence (IF) staining reagent were purchased from Servicebio (Wuhan, China). The GAPDH solution was obtained from Bioss (Beijing, China) and Bioworld (Illinois, USA). The HRP- (horseradish peroxidase-) labeled goat anti-Rat IgG solution and the HRP-labeled goat anti-rabbit IgG solution were obtained from Epizyme (Shanghai, China). The ECL (enhanced chemiluminescence) substrate and PVDF (polyvinylidene fluoride) membrane were purchased from Merck Millipore (Darmstadt, Germany). The 0.05 M PB (phosphate buffer) solution (250 ml) consisted of 0.6555 g NaH2PO4·2H2O and 7.2495 g Na2HPO4·12H2O dissolved in distilled water, with a constant volume of 250 ml. NaH2PO4·2H2O and Na2HPO4·12H2O were obtained from Solarbio (China, Beijing).

Radioactive counts were measured using the Gamma counter from Capintec Inc. (USA). The phosphor autoradiography images were captured and analyzed using Cyclone Plus Scanner (PerkinElmer, Life Sciences, USA). The membrane was scanned with the Tanon 5200 imaging system scanner (Tanon, Shanghai, Beijing).

2.2. Radiochemistry

2.2.1. Preparation of the Radio Probe. The preparation of the ^{125}I-labeled probe was performed according to reference (36). Briefly, 0.05 M PB solution (100 μl), IL-27Rα mAb (12 μg) or rIL-27 (8 μg), and Na^{125}I (11.9 MBq) were mixed in the tube with iodogen at room temperature for 15 minutes. The tube was gently shaken every 3-4 minutes. 150 μl 0.05 M PB was added to the tube and allowed to stand at room temperature for 10 minutes. 200 μl 5% BSA reagent (containing bromophenol blue) was added to the tube and gently shaken. The mixture was then added to the Sephadex G-25M PD10 column, followed by elution with 0.01 M PB solution. The eluent was collected in a tube (0.5 ml for each

tube), and the radioactive count of 10 μl eluent of each tube was measured by the Gamma counter.

$$\begin{aligned}&\text{Radiochemical yield}\\&= (\text{radioactivity of the first peak})/\\&\quad(\text{summed radioactivity counts for each tube}).\end{aligned} \tag{1}$$

Radiochemical purity was detected following the protocol [19]. Briefly, 2 μl of the radio probe was added to the filter paper (2 cm to the bottom). The bottom of the paper was then immersed in 0.9% saline and methanol solution (1 : 2, *v*/*v*). After 40 min, the paper was cut into slices (1 cm) and the radioactive count was measured using a Gamma counter. Radiochemical purity = (radioactivity near the sample)/(total radioactivity of every slice).

2.2.2. In Vitro Stability Study. The radio probe (12.5 μl) was dissolved in saline (100 μl) or mouse serum (100 μl), and the mixture was kept at 37°C for a period of time. At 1, 12, and 24 h, 2 μl of the sample was taken and analyzed to observe the change in radiochemical purity.

2.2.3. Determination of Lipophilicity. ^{125}I-rIL-27 (0.2 μl, 4.08×10^{-4} MBq) was diluted in 1 M HEPES buffer (500 μl) and mixed with n-octanol (500 μl) for 30 min, followed by centrifugation for 10 min with 14000 × g. Subsequently, aliquots of the n-octanol and water phases (400 μl) were taken out and then centrifuged again. Finally, the radioactive count of each phase (100 μl) was measured by the Gamma counter and the octanol/water partition coefficient (log $D_{o/w}$) was calculated.

2.3. Cell Assays. Cell assays were performed using isolated mouse model spleen cells on day 10 after transplantation. Briefly, the mouse model spleen was isolated and pressed on mesh 200. The cells were then treated with red blood cell lysis buffer, washed with PBS, and finally suspended in RPMI-1640 medium. Cells were cultured in 48-well plates for 2 h with each well 1×10^6 cells in 200 μl RPMI 1640 medium and used for further studies after attachment.

2.3.1. Competition Study. For competition binding assay, nonlabeled anti-IL-27Rα mAb (0 to 71.4 μM) was incubated with alloreactive spleen cells for 1 h before adding 147.09 nM ^{125}I-rIL-27. Cells were washed with cold PBS buffer twice, and the supernatant was discarded. The activity bound to the cells was measured by a Gamma counter. B/B_0 was described as the ratio of radioactive counts with nonlabeled anti-IL-27Rα mAb to radioactive counts without nonlabeled anti-IL-27Rα mAb. The inhibition constant (K_i value) was calculated in GraphPad Prism software.

2.3.2. Saturation Study. ^{125}I-rIL-27 (3.68 to 147.09 nM) was incubated with spleen cells for 2 h at 37°C to obtain the total binding activity of ^{125}I-rIL-27. To test nonspecific binding, cells were pretreated for 1 hour with 10.46 μM nonlabeled rIL-27.

After incubation with ^{125}I-rIL-27, cells were washed twice with cold PBS buffer and radioactivity was measured with the Gamma counter. Maximum binding capacity (B_{max}) and dissociation constant [37] were calculated in the GraphPad Prism software. Specific binding was the value of total binding minus nonspecific binding.

2.4. Animal Experiments In Vivo. All animal experiments were performed according to the ARRIVE guidelines. The protocol was approved by the Shandong University Animal Care and Use Committee with the corresponding ethical approval code (LL-201602040, 2016-2022). Female BALB/c mice (H-2^d) and C57BL/6 mice (H-2^b) were purchased from Vital River Laboratory Animal Technology (Beijing, China) and housed in standard conditions with free access to water and standard food.

2.4.1. Animal Models. To establish the skin transplantation model, C57BL/6 mice and BALB/c mice were used as allogeneic and syngeneic transplant skin graft donors, respectively. BALB/c mice were recipients. Briefly, surgery was performed under anesthesia with 0.6% pentobarbital sodium (0.1 ml/10 g body weight) under sterility conditions. The mucous membrane and blood vessel of the graft were removed, and then, the graft was cut into a circle with 1 cm diameter. Then, remove the skin of the recipients on the right shoulder and transfer the graft to the recipients. Finally, petrolatum gauze was placed on the graft and covered with bandage. Acute rejection occurred on day 7 after transplantation when the bandage with the escharotic area was removed greater than 50%.

2.4.2. Blood Clearance Assay. At 1 h, 2 h, 6 h, 12 h, and 24 h after radio probe injection, mice were anesthetized with 0.6% pentobarbital sodium solution. Then, 5 μl blood was drawn from the tail vein. The activity of the radio probe that remained in the blood was counted by the Gamma counter. Each mouse was weighted, and the radio probe concentration in the blood (ng/μl) was calculated using 78 ml/kg as a blood factor. The AUCs (area under the curves) of ^{125}I-rIL-27 in 24 h and ^{125}I-anti-IL-27Rα mAb in 48 h were obtained using the GraphPad Prism software. Blood clearance (CL, μl/h) was calculated as the dose/AUC with the study referred to [38].

2.4.3. Dynamic Phosphor Autoradiography. Mice were divided into an allogroup, a syngroup, and a blocking group according to the allogeneic, syngeneic, and allogeneic transplantation model with specific antibody blocking. After being fed 3% NaI solution for 24 h, 60 μg nonlabeled IL-27Rα mAb was injected into the blocking group. One hour later, all mice were injected with ^{125}I-rIL-27 (0.37 MBq) and ^{125}I-anti-IL-27Rα mAb (0.37 MBq) on day 9 after transplantation, respectively. Mice were anesthetized and scanned with the Cyclone Plus Scanner. ROIs (regions of interest) were quantified using OptiQuant Image Analysis software and presented as digital light units per square millimeter (DLU/mm^2).

2.4.4. Ex Vivo Biodistribution. Three groups of mice (allogroup, syngroup, and blocking group, $n = 3$ for each group) were sacrificed 24 h after intravenous injection of a

radio probe (0.08 MBq in 200 μl of 0.01 M PB). Organs or tissues of interest, including blood, liver, lung, kidney, spleen, control skin, and graft, were excised and weighed. The activity was measured by a Gamma counter, and the uptake of the radio probe was expressed as the percentage of injected dose per gram (%ID/g). The T/NT (target/non-target) ratio was calculated by dividing the %ID/g of the target graft to that of the control skin (opposite site), while T/B (target/blood) was %ID/g of the target graft to that of the blood.

2.4.5. H&E Staining and Immunofluorescence Staining. On day 10 after transplantation, the grafts were collected and histological sections were prepared. H&E staining and immunofluorescence staining were performed following the staining kit protocols. The image was obtained under an optical microscope. Briefly, in H&E staining, sections were covered with hematoxylin for 5 min. After applying 1% acid ethanol reagent for 5 seconds, sections were covered with a blue promotor solution for 5 seconds. The sections were then covered with eosin solution for 10 minutes. Between each step, distilled water was used to wash out excess buffer. In IF staining, sections were treated with EDTA antigen repair buffer (pH 9.0) and blocked with BSA for 30 min. Anti-IL-27Rα Ab was then diluted in PBS (1 : 200) and added to the section at 4°C, overnight. Sections were washed with PBS and covered with a second antibody for 1 hour. Later, sections were washed with PBS and the FITC regent (green) was added to the sections. The sections were then washed with TBST and covered with tissue autofluorescence quencher regent for 5 min. The excess regent was then washed with distilled water for 10 min. The sections were discarded excess liquid and incubated with DAPI regent (blue) for 10 min at room temperature. Finally, the sections were washed with PBS and then enclosed with antifade mounting medium.

2.4.6. Western Blot. After 10 d of transplantation, the grafts were separated, lysed, and reacted with SDS loading buffer. Electrophoresis was performed, and the protein was transferred to the PVDF membrane. The target membrane was then treated with blocking buffer and then covered with anti-IL-27Rα mAb solution and a GAPDH solution overnight. The membrane was then washed with TBST buffer and covered with HRP-labeled goat anti-rat IgG solution and HRP-labeled goat anti-rabbit IgG solution, respectively. Finally, the membrane was washed with TBST buffer, followed by ECL substrate covering. The band was scanned with the Tanon 5200 imaging system scanner and analyzed with ImageJ software.

2.5. Statistical Analysis. All data were quoted as mean ± standard deviation (mean ± SD), and each data point emerged from 3 independent experiments. Comparisons between two groups were analyzed using the unpaired Student t-test. The correlation between DLU/mm^2 of ^{125}I-rIL-27 and the expression of IL-27Rα was calculated using a correlation assay. The statistically significant level was established at $p < 0.05$.

3. Results

3.1. Radiochemistry. The labeling yields of ^{125}I-rIL-27 and ^{125}I-anti-IL-27Rα mAb were 84.4% and 99.0%, respectively. The radiochemistry purity of these radio probes was 93.3% and 95.3%. The stabilities of the ^{125}I-rIL-27 and ^{125}I-anti-IL-27Rα mAb were more than 90% in saline and mouse serum even after 24 h (supplement Figure 1), respectively. The results showed that the ^{125}I-rIL-27 and ^{125}I-anti-IL-27Rα mAb were quite stable. The log $D_{o/w}$ values for ^{125}I-rIL-27 were -1.18 ± 0.23, which means that ^{125}I-rIL-27 has a hydrophilic character.

3.2. Cell Binding Assays

3.2.1. Saturation. Typical saturation graphs obtained after incubation of 1×10^6 cells with ^{125}I-rIL-27 are shown in Figures 1(a) and 1(b). The B_{max} values of ^{125}I-rIL-27 in alloreactive and synreactive splenocytes were 2545 cpm/10^6 cells and 1607 cpm/10^6 cells, respectively. Furthermore, K_d values were found to be 48.59 nM and 49.04 nM for allo- and synreactive splenocytes, respectively.

3.2.2. Competition. Figure 1(c) shows that the binding of ^{125}I-rIL-27 decreased as anti-IL-27Rα mAb increased. Using the K_d value of ^{125}I-rIL-27 from the saturation assay, the determination of the K_i value was 769.9 nM using the Cheng-Prusoff equation.

3.3. Small Animal In Vivo Experiments

3.3.1. Blood Clearance Assay. To understand how fast ^{125}I-rIL-27 cleared in vivo, a blood clearance assay was performed. Blood clearance was represented as a clearance value. The allogroup showed a significantly lower concentration of ^{125}I-rIL-27 than ^{125}I-anti-IL-27Rα mAb in the blood (0.450 ± 0.095 vs. 0.808 ± 0.089 ng/μl, $p < 0.01$), and the syngroup showed the same pattern (0.342 ± 0.281 vs. 0.8967 ± 0.0753 ng/μl, $p < 0.05$) at 24 h after injection. The AUC was shown in Figure 2, and the retention of ^{125}I-rIL-27 in the blood was shorter than that of ^{125}I-anti-IL-27Rα mAb in the allogroup (35.52 vs. 53.17 h·ng/μl) at 24 h. The syngroup showed shorter retention of ^{125}I-rIL-27 than ^{125}I-anti-IL-27Rα mAb (31.53 vs. 52.65 h·ng/μl) at 24 h. ^{125}I-rIL-27 demonstrated faster blood clearance compared with ^{125}I-anti-IL-27Rα mAb in the allogroup (13.20 vs. 9.43 μl/h) and syngroup (14.87 vs. 9.53 μl/h) at 24 h. All these suggested a significantly faster blood clearance of ^{125}I-rIL-27 than ^{125}I-anti-IL-27Rα mAb in allograft rejection model mice.

3.3.2. Dynamic Whole-Body Phosphor Autoradiography Imaging. To investigate ^{125}I-rIL-27 imaging in vivo, we performed dynamic whole-body phosphor autoradiography imaging. As shown in Figure 3(a), high uptake of ^{125}I-rIL-27 was obtained in the allogeneic graft (DLU/mm^2: 434241.58 ± 53524.20) at 6 h after intravenous injection and then reached a plateau up to 24 h (DLU/mm^2: 163603.46 ± 56677.03), while lower uptake was obtained in the syngeneic graft (DLU/mm^2: 66401.60 ± 29698.30)

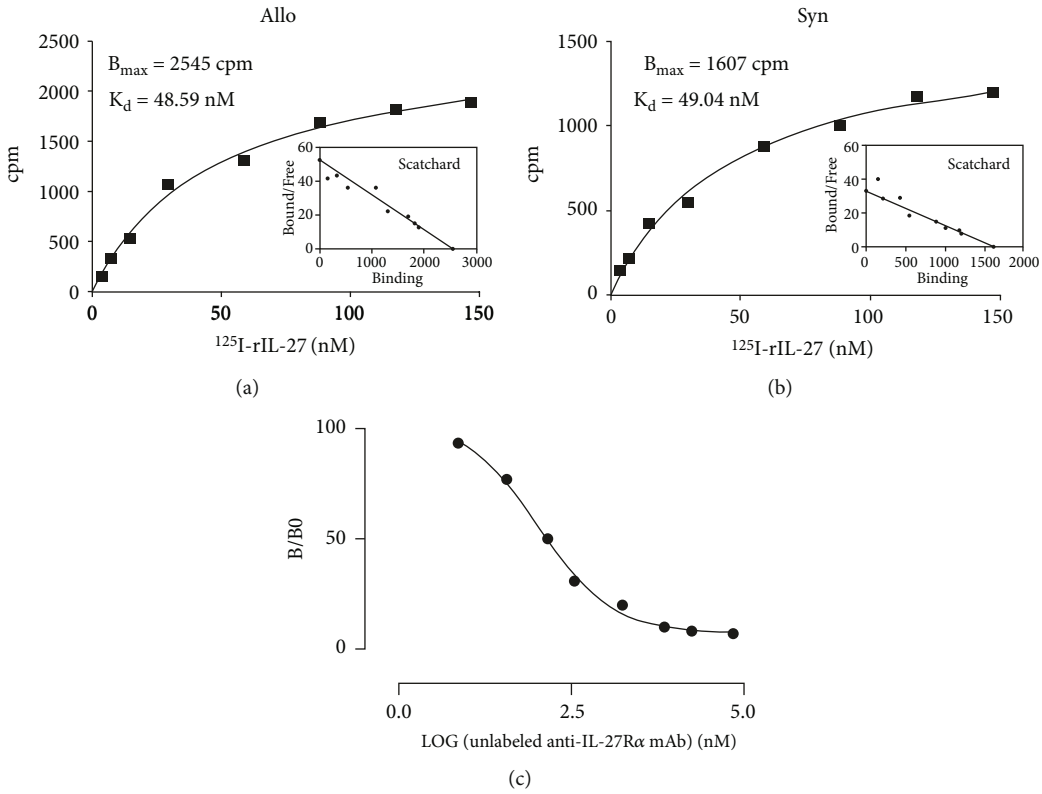

Figure 1: Binding assay of 125I-rIL-27 in vitro.

	Group	AUC (h∗ng/μl)	CL (μl/h)
^{125}I-rIL-27	Allo	35.52	13.20
	Syn	31.53	14.87
^{125}I-anti-IL-27Rα mAb	Allo	53.17	9.43
	Syn	52.65	9.53

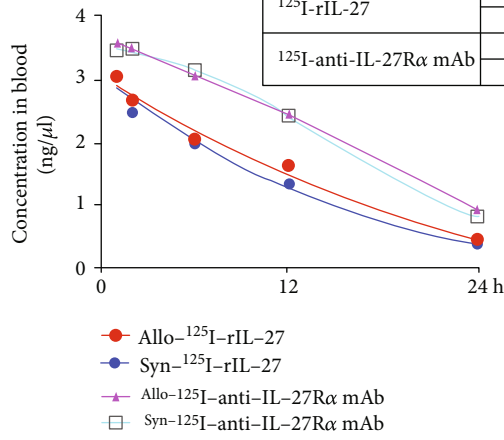

Figure 2: Blood clearance assay.

($p < 0.01$). The in vivo specificity of ^{125}I-rIL-27 was confirmed by blocking studies using excess unlabeled anti-IL-27Rα mAb (DLU/mm^2: 68252.033 ± 38373.75). Ex vivo autoradiography apparently showed a high accumulation of activity in the allograft. A similar result of ^{125}I-anti-IL-27Rα mAb was observed at 48 h, and the uptake of ^{125}I-anti-IL-27Rα mAb in the allogeneic graft was also higher than in the syngeneic graft (Figure 3(b)). However, the image using ^{125}I-rIL-27 in the allogeneic graft exhibited a lower background compared to the image with that using ^{125}I-anti-IL-27Rα mAb. These indicated that ^{125}I-rIL-27 could target the allograft specifically and produce better images with high contrast and low background.

3.3.3. Biodistribution Assay. To gain first insight into the potential relevance of ^{125}I-rIL-27 for transplantation imaging, a biodistribution assay was performed using skin transplantation mice. Biodistribution data for ^{125}I-rIL-27 was shown in Figure 4(a). Higher uptake was observed in the allogeneic skin graft compared to that in the syngeneic group (Figure 4(b)).

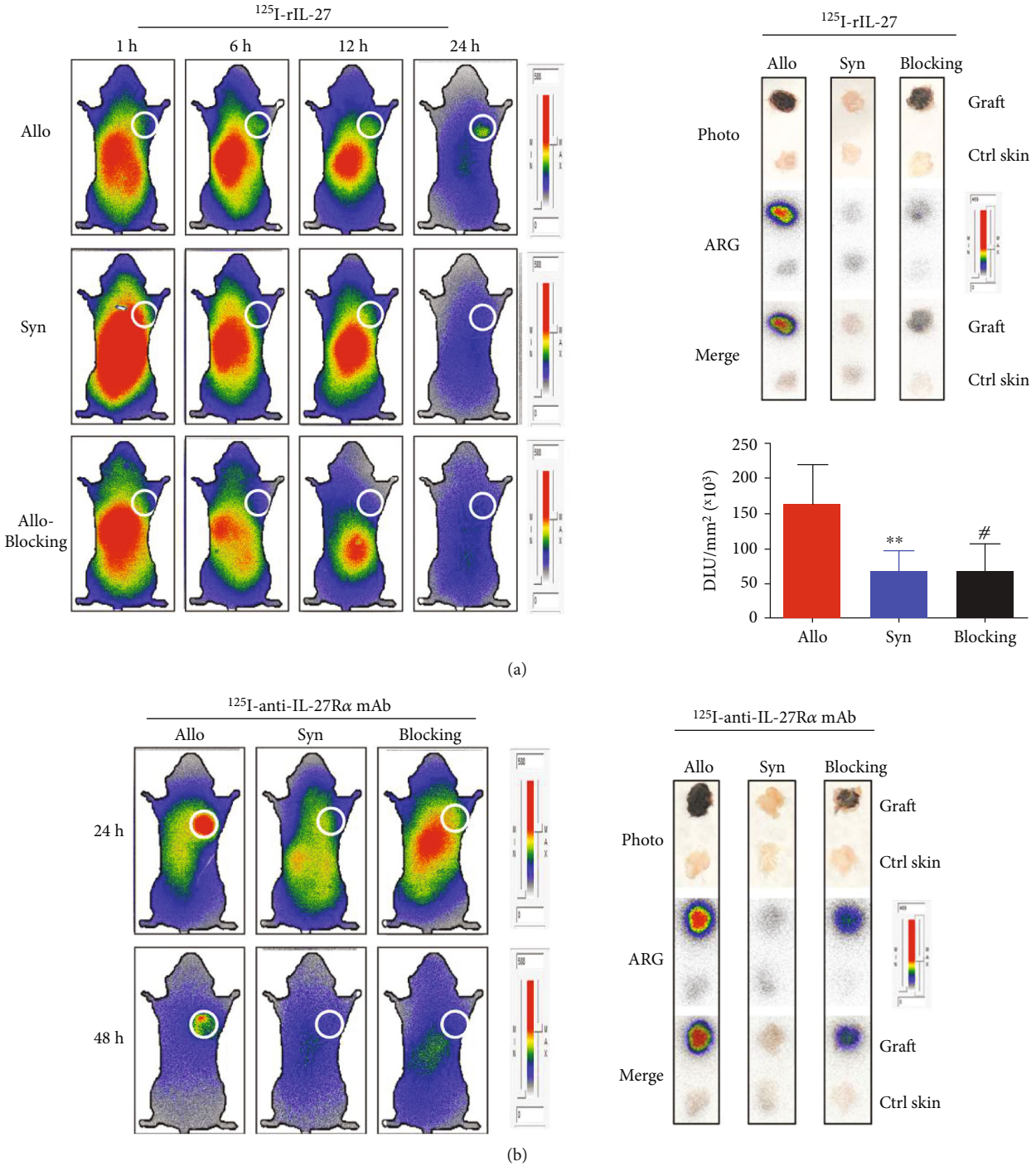

Figure 3: Dynamic whole-body phosphor autoradiography imaging assay.

The uptake of the activity of ^{125}I-rIL-27 in the allograft was higher than that in the syngraft (%ID/g: 5.648 ± 1.735 vs. 1.751 ± 0.967, $p < 0.01$). The T/NT ratio and the T/B ratio increased significantly in the allogroup compared to the syngroup in Figures 4(b) and 4(c).

More interestingly, compared to ^{125}I-anti-IL-27Rα mAb, fewer ^{125}I-rIL-27 in the blood were obtained 24 h after injection not only in the allogroup (%ID/g: 6.960 ± 0.754 vs. 4.083 ± 0.710, $p < 0.01$) but also in the syngroup (%ID/g: 6.090 ± 0.508 vs. 3.230 ± 1.835, $p < 0.05$). Furthermore, the activity uptake of ^{125}I-rIL-27 was also lower than that of ^{125}I-anti-IL-27Rα mAb in the liver, lung, kidney, and spleen. These indicated that ^{125}I-rIL-27 could specifically recognize IL-27Rα overexpressed in the allograft and have favorable imaging with low background.

3.3.4. IL-27Rα Expression in the Rejection of Allograft. To study the correlation between the accumulation of activity of ^{125}I-rIL-27 and the expression of IL-27Rα in the rejection

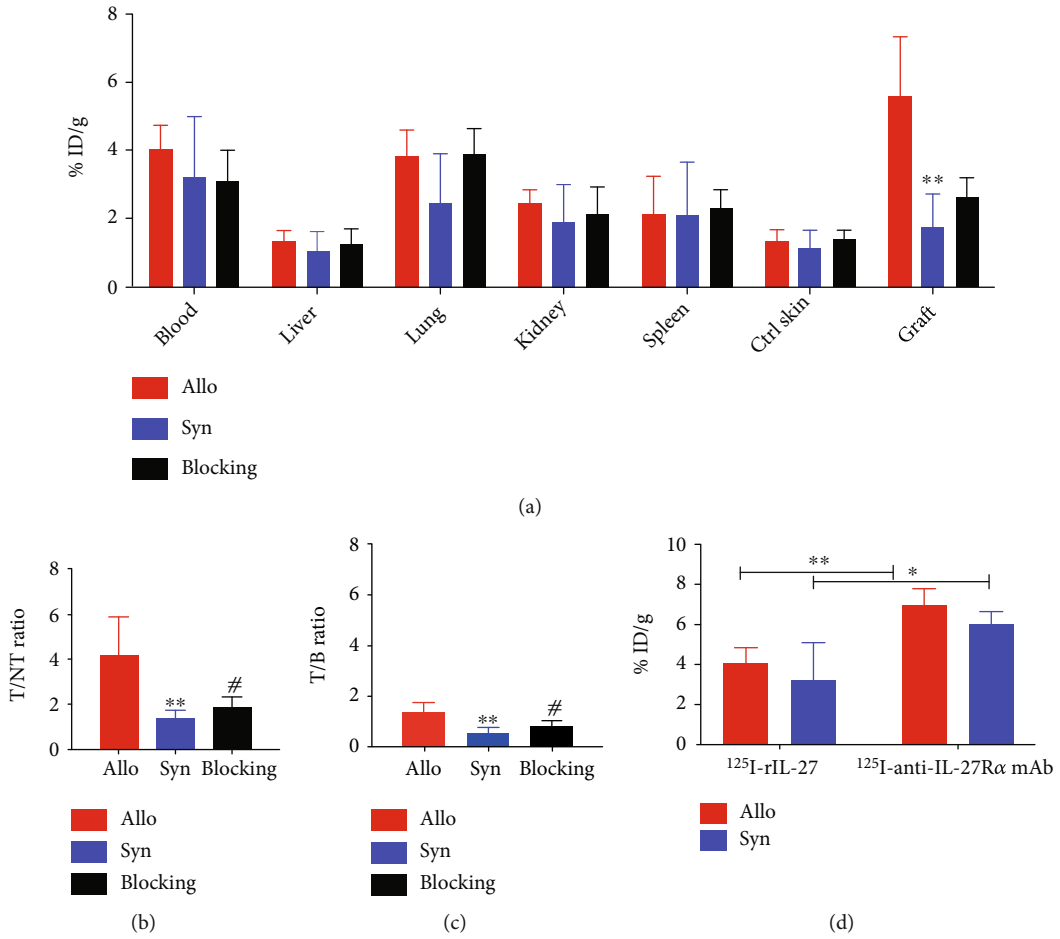

Figure 4: Biodistribution study on day 10 after transplantation.

of the allograft, IF staining was performed on day 10 after transplantation to determine the IL-27Rα expression.

HE staining in Figure 5(a) confirmed that a severe rejection response occurred in allogeneic graft, while mild inflammation occurred in syngeneic graft. IL-27Rα expression was obviously higher in the allograft (Figure 5(b)). The accumulation of activity (DLU/mm^2) in the graft had a positive correlation with IL-27Rα expression (Figure 5(c)). Fluorescence imaging also confirmed the higher expression of IL-27Rα on the surface of infiltrated cells of rejecting the allograft (Figure 5(d)). All of these suggested that ^{125}I-rIL-27 could specifically bind the IL-27Rα in the allograft, monitoring acute rejection.

4. Discussion

Early acute allorejection is usually more responsive to allograft transplant therapy, and therefore, timely detection of acute rejection could benefit the prognosis [39]. Up to now, molecular imaging with specific radio probes was a promising method responsible for the detection of allograft rejection [23]. Recently, IL-27, a pleiotropic cytokine with proinflammatory properties, was reported with enhanced antitumor and antivirus activities and participated in the rejection response [40–42]. IL-27 could promote the infiltration of CD4$^+$T cells and CD8$^+$T cells in the tumor and upregulate IFN-γ, granzyme B, and perforin production, resulting in an improved antitumor effect of T cells [11]. Moreover, IL-27 could also boost NK cells proliferation and cytotoxic activity synergistically with IL-15/IL-18 [43]. All of these indicated that IL-27/IL-27R was a promising target in the proinflammatory immune response. IL-27Rα, the subunit of the IL-27 receptor, which was also expressed in T cells and macrophages, had the highest expression during the acute rejection period in the allograft [44–46]. In our previous study, ^{125}I-anti-IL-27Rα mAb has been found with high specificity towards IL-27Rα [19]. However, it had limitations in nonspecific binding to Fc recognition, slow metabolism, and clearance, compared to a small antibody fragment or ligand [31, 47]. Therefore, a small radio probe could provide better imaging with a low background.

The cytokine was a small ligand of the cytokine receptor that was expressed on the surface of effector cells [47]. Many radio cytokine probes have already been applied in target imaging [48–51]. Radiolabeled IL-2 probes were used in clinics for the targeted detection of lymphocytic infiltration in transplantation and atherosclerotic plaque [48, 49]. Glaudemans et al. found that symptomatic plaques with high CD3$^+$ cell infiltration had a significant uptake of ^{99m}Tc-HYNIC-IL-2 and the lung of the rejection patient had

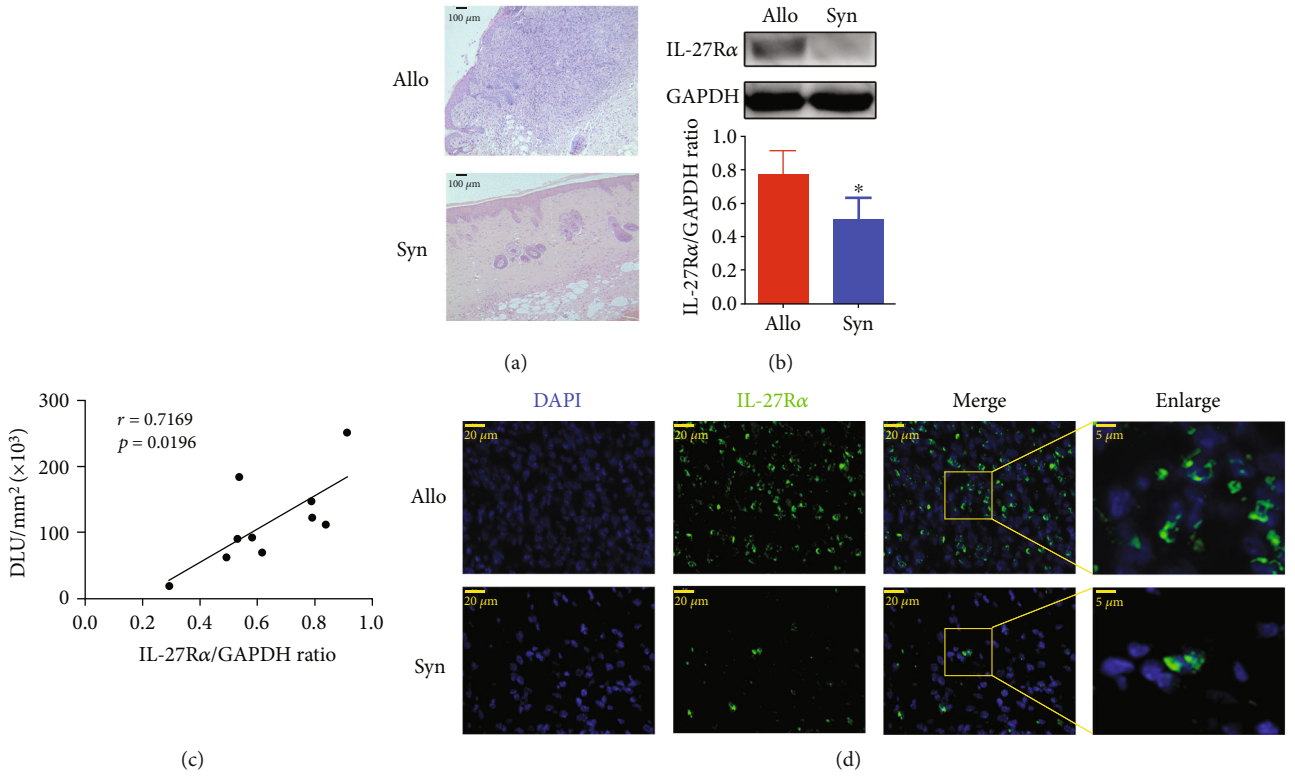

Figure 5: H&E staining and IL-27Rα expression.

increased ^{99m}Tc-HYNIC-IL-2 uptake. In their researches, no side effects were found with the administration of ^{99m}Tc-HYNIC-IL-2. We also developed the ^{125}I-rIL-27 targeted radio probe with high radiochemical purity. Because the Sephadex G-25M PD10 column allowed for rapid group separation of high-molecular-weight substances form low-molecular-weight substances, the radio probe which has high molecular weight would be eluted first. The radioactive probes were easier to observe because they contain proteins that could be stained blue with bromophenol blue. Meanwhile, the radio count assay of the elution would help to confirm the radio probe. We found that ^{125}I-rIL-27 would keep stable for 24 hours after synthesis using the paper chromatography method. This is a traditional method to determine radiochemical purity and has reproducible and accurate radio counts [52]. When the radio compound is not dissociated, the radio compound swims slowly in the medium because of its large molecular weight. Therefore, the place where the sample was had the highest radioactivity count. And when the radio compound dissociated, free iodine 125 would produce a higher radioactivity count on the upper paper. This method will help to demonstrate the radiochemical purity and stability of the radio probe. Also, we also found that this radio probe had no side effects in the mouse model.

The in vitro experiment showed that our ^{125}I-rIL-27 had a specific binding to IL-27Rα on the spleen cells. However, the binding ability and affinity of ^{125}I-rIL-27 were lower than those of ^{125}I-anti-IL-27Rα mAb. This could be due to the fact that ^{125}I-anti-IL-27Rα mAb has nonspecific binding of the Fc fragment. Matsushima et al. developed ^{125}I-labeled IL 1β in a human large granular lymphocyte cell line (YT cells), and this radio probe showed a higher affinity of 0.1 nM (K_d value) compared to our probe [53]. It may be due to the different receptor expressions of the cells. Furthermore, the isolation process of spleen cells may also result in some loss of receptors [54].

In the imaging of [^{124}I] I-F8-IL10, it was suggested that the target area had the highest uptake and target-to-background ratios at 24 h after injection of the radio probe [35]. Therefore, we carried out biodistribution and blood clearance of ^{125}I-rIL-27 within 24 h after radio probe injection. In the blood clearance assay, ^{125}I-rIL-27 showed faster blood clearance than ^{125}I-anti-IL-27Rα, which could be due to different levels of cytokines and antibody glycosylation, which influence receptor recognition and blood clearance [55]. The blood clearance assay showed a shorter retention of ^{125}I-anti-IL-27Rα in the blood compared to monoclonal antibody, which could be due to recognition of Fc [56]. The whole-body phosphor autoradiography imaging demonstrated that the allograft had more activity accumulation than the syngeneic graft, and this accumulation could be blocked by excess of anti-IL-27Rα mAb. A lower background was also observed at 24 h in the ^{125}I-rIL-27 group compared with ^{125}I-anti-IL-27Rα. The tumor necrosis factor superfamily (TNFSF) contains CD40L, FasL, TRAIL (TNF-related apoptosis-inducing ligand), LiGHT, VEGF (vascular endothelial growth factor), lymphotoxin alpha, lymphotoxin beta, and lymphotoxin alpha1/beta2, which could be fused with the F8 antibody for tumor targeting. In biodistribution,

it was suggested that the %ID/g of ^{125}I-rIL-27 in the allograft was similar to that of F8-TRAILtrunc, lower than that of F8-CD40L, and higher than that of other TNFSF in the tumor [57]. The reason may be the different expressions and affinity of different receptors for the receptors. The %ID/g of ^{125}I-rIL-27 (47.8 KDa) in the blood was higher than that of F8-TNFSF, F8-IL-10 (18.6 KDa), and ^{99m}Tc-VEGF$_{165}$ (16 KDa), probably due to the lower molecular weight of other cytokines [50]. However, the activity of ^{125}I-rIL-27 in the blood was much lower compared to that of ^{125}I-anti-IL-27Rα (155KDa), possibly caused by the nonspecific Fc binding of ^{125}I-anti-IL-27Rα. The uptake of ^{125}I-rIL-27 in the lung was higher than that in other organs, except graft and blood. This could be due to the enrichment of immune cells overexpressed with IL-27Rα in the lung. Meanwhile, blood pollution should also be considered. The accumulation of activity in the kidney was found to be higher than in the liver, which may be due to the hydrophilic character of ^{125}I-rIL-27. Furthermore, it was also found that the accumulation of ^{125}I-rIL-27 had a close correlation with the expression of IL-27Rα of the graft. All of these indicated that ^{125}I-rIL-27 was a promising radiotracer that could specifically target IL-27Rα for the imaging of acute rejection allograft with faster blood clearance and low background, compared with ^{125}I-anti-IL-27Rα mAb.

5. Conclusions

In this study, the acute rejection of allograft could be detected by targeting IL-27Rα in allograft specifically with ^{125}I-rIL-27. The rejecting allograft had higher specific ^{125}I-rIL-27 uptake than nonrejecting syngeneic graft, and the accumulation of activity was in close correlation with the expression of IL-27Rα of the graft. More importantly, low background and rapid clearance were obtained for ^{125}I-rIL-27 compared with ^{125}I-anti-IL-27Rα mAb. Imaging with this small radio probe could be a promising strategy for noninvasive monitoring of IL-27Rα-overexpressed rejecting allograft.

Data Availability

All data included in this study are available upon request by contact with the corresponding author.

Additional Points

Statement. A preprint has previously been published [58].

Conflicts of Interest

The authors have no conflicts of interest to disclose.

Authors' Contributions

Shanshan Zhao and Guihua Hou designed the studies. Shanshan Zhao and Qian Liu carried out the study, including data collection and data analysis. Shanshan Zhao, Qian Liu, Feng Gao, and Guihua Hou wrote the manuscript. All authors read and approved the final manuscript.

Acknowledgments

The author thanks the Translational Medicine Core Facility of Shandong University for the consultation and availability of instruments that supported this work. This research was funded by grants from the Natural Science Foundation of Shandong Province (grant numbers ZR2019MH019).

Supplementary Materials

The figure showed the radiochemistry of ^{125}I-rIL-27 and ^{125}I-anti-IL-27Rα, including labeling yields and stabilities. The labeling yields were calculated by the radio counts of the elution. Stabilities were performed by the paper chromatography method. *(Supplementary Materials)*

References

[1] A. Loupy and C. Lefaucheur, "Antibody-Mediated Rejection of Solid-Organ Allografts," *New England Journal of Medicine*, vol. 379, no. 26, pp. 2579–2582, 2018.

[2] R. Grenda and P. Kaliciński, "Combined and sequential liver-kidney transplantation in children," *Pediatric Nephrology*, vol. 33, no. 12, pp. 2227–2237, 2018.

[3] M. Jalalzadeh, N. Mousavinasab, S. Peyrovi, and M. H. Ghadiani, "The impact of acute rejection in kidney transplantation on long-term allograft and patient outcome," *Nephro-Urology Monthly*, vol. 7, no. 1, article e24439, 2015.

[4] M.-K. Tsai, F.-L. L. Wu, R. Lai, C.-Y. Lee, R.-H. Hu, and P.-H. Lee, "Decreased acute rejection and improved renal allograft survival using sirolimus and low-dose calcineurin inhibitors without induction therapy," *International Journal of Artificial Organs*, vol. 32, no. 6, pp. 371–380, 2009.

[5] I. O. Peshkova, T. Aghayev, A. R. Fatkhullina et al., "IL-27 receptor-regulated stress myelopoiesis drives abdominal aortic aneurysm development," *Nature Communications*, vol. 10, no. 1, pp. 5046–5046, 2019.

[6] G. Yao, J. Qi, J. Liang et al., "Mesenchymal stem cell transplantation alleviates experimental Sjögren's syndrome through IFN-β/IL-27 signaling axis," *Theranostics*, vol. 9, no. 26, pp. 8253–8265, 2019.

[7] Z. Huang, J. Zak, I. Pratumchai et al., "IL-27 promotes the expansion of self-renewing CD8(+) T cells in persistent viral infection," *The Journal of Experimental Medicine*, vol. 216, no. 8, pp. 1791–1808, 2019.

[8] D. Bastian, Y. Liu, Y. Wu et al., "IL-27 receptor signaling on T cells augments GVHD severity through enhancing Th1 responses," *Journal of Immunology Research and Therapy*, vol. 3, no. 1, pp. 151–157, 2018.

[9] Q. Wang, H. Ning, H. Peng et al., "Tristetraprolin inhibits macrophage IL-27-induced activation of antitumour cytotoxic T cell responses," *Nature Communications*, vol. 8, no. 1, pp. 867–867, 2017.

[10] G. W. Jones, D. G. Hill, A. Cardus, and S. A. Jones, "IL-27: a double agent in the IL-6 family," *Clinical and Experimental Immunology*, vol. 193, no. 1, pp. 37–46, 2018.

[11] J. Zhu, J.-Q. Liu, M. Shi et al., "IL-27 gene therapy induces depletion of Tregs and enhances the efficacy of cancer immunotherapy," *JCI insight*, vol. 3, no. 7, article e98745, 2018.

[12] C. Petes, C. Wynick, C. Guzzo et al., "IL-27 enhances LPS-induced IL-1β in human monocytes and murine

macrophages," *Journal of Leukocyte Biology*, vol. 102, no. 1, pp. 83–94, 2017.

[13] P. Kumar, K. Rajasekaran, A. Nanbakhsh, J. Gorski, M. S. Thakar, and S. Malarkannan, "IL-27 promotes NK cell effector functions via Maf-Nrf2 pathway during influenza infection," *Scientific Reports*, vol. 9, no. 1, article 4984, 2019.

[14] M. Benzimra, G. L. Calligaro, and A. R. Glanville, "Acute rejection," *Journal of Thoracic Disease*, vol. 9, no. 12, pp. 5440–5457, 2017.

[15] M. Gaignage, R. G. Marillier, P. M. Cochez et al., "The TLR7 ligand R848 prevents mouse graft-versus-host disease and cooperates with anti-interleukin-27 antibody for maximal protection and regulatory T-cell upregulation," *Haematologica*, vol. 104, no. 2, pp. 392–402, 2019.

[16] C. Petes, M. K. Mariani, Y. Yang, N. Grandvaux, and K. Gee, "Interleukin (IL)-6 inhibits IL-27- and IL-30-mediated inflammatory responses in human monocytes," *Frontiers in Immunology*, vol. 9, p. 256, 2018.

[17] S.-L. Qiu, M.-C. Duan, Y. Liang et al., "Cigarette smoke induction of interleukin-27/WSX-1 regulates the differentiation of Th1 and Th17 cells in a smoking mouse model of emphysema," *Frontiers in Immunology*, vol. 7, pp. 553–553, 2016.

[18] J. Xu, D. Wang, C. Zhang et al., "Alternatively expressed genes identified in the CD4+ T cells of allograft rejection mice," *Cell Transplantation*, vol. 20, no. 2, pp. 333–350, 2011.

[19] S. Zhao, D. Shi, C. Su et al., "IL-27Rα: a novel molecular imaging marker for allograft rejection," *International Journal of Molecular Sciences*, vol. 21, no. 4, article 1315, 2020.

[20] A. Sharfuddin, "Renal Relevant Radiology: Imaging in Kidney Transplantation," *Clinical Journal of the American Society of Nephrology*, vol. 9, no. 2, pp. 416–429, 2014.

[21] A. Roden, D. Aisner, T. Allen et al., "Diagnosis of acute cellular rejection and antibody-mediated rejection on lung transplant biopsies: a perspective from members of the pulmonary pathology society," *Archives of Pathology & Laboratory Medicine*, vol. 141, pp. 437–444, 2017.

[22] Y. Huang, E. A. Sadowski, N. S. Artz et al., "Measurement and comparison of T1 relaxation times in native and transplanted kidney cortex and medulla," *Journal of magnetic resonance imaging: JMRI*, vol. 33, no. 5, pp. 1241–1247, 2011.

[23] R. Köhnke, D. Kentrup, K. Schütte-Nütgen et al., "Update on imaging-based diagnosis of acute renal allograft rejection," *American Journal of Nuclear Medicine and Molecular Imaging*, vol. 9, no. 2, pp. 110–126, 2019.

[24] T. Liao, Y. Zhang, J. Ren et al., "Noninvasive quantification of intrarenal allograft C4d deposition with targeted ultrasound imaging," *American Journal of Transplantation*, vol. 19, no. 1, pp. 259–268, 2019.

[25] D. M. Xu, M. Chen, F. D. Zhou, and M. H. Zhao, "Risk factors for severe bleeding complications in percutaneous renal biopsy," *The American Journal of the Medical Sciences*, vol. 353, no. 3, pp. 230–235, 2017.

[26] H. Chi, B. E. Hansen, W. Y. Tang et al., "Multiple biopsy passes and the risk of complications of percutaneous liver biopsy," *European Journal of Gastroenterology & Hepatology*, vol. 29, no. 1, pp. 36–41, 2017.

[27] A. C. Freise, K. A. Zettlitz, F. B. Salazar, X. Lu, R. Tavaré, and A. M. Wu, "ImmunoPET imaging of murine CD4+ T cells using anti-CD4 Cys-diabody: effects of protein dose on T cell function and imaging," *Molecular Imaging and Biology*, vol. 19, no. 4, pp. 599–609, 2017.

[28] S. Mall, N. Yusufi, R. Wagner et al., "Immuno-PET imaging of engineered human T cells in tumors," *Cancer Research*, vol. 76, no. 14, pp. 4113–4123, 2016.

[29] H. Sun, G. Yang, T. Liang et al., "Non-invasive imaging of allogeneic transplanted skin graft by 131I-anti-TLR5 mAb," *Journal of Cellular and Molecular Medicine*, vol. 18, no. 12, pp. 2437–2444, 2014.

[30] P. Berraondo, M. F. Sanmamed, M. C. Ochoa et al., "Cytokines in clinical cancer immunotherapy," *British Journal of Cancer*, vol. 120, no. 1, pp. 6–15, 2019.

[31] E. B. Ehlerding, H. J. Lee, D. Jiang et al., "Antibody and fragment-based PET imaging of CTLA-4+ T-cells in humanized mouse models," *American Journal of Cancer Research*, vol. 9, no. 1, pp. 53–63, 2019.

[32] T. Ying, Y. Feng, Y. Wang, W. Chen, and D. S. Dimitrov, "Monomeric IgG1 Fc molecules displaying unique Fc receptor interactions that are exploitable to treat inflammation-mediated diseases," *MAbs*, vol. 6, no. 5, pp. 1201–1210, 2014.

[33] S. V. Hartimath, O. Draghiciu, S. van de Wall et al., "Noninvasive monitoring of cancer therapy induced activated T cells using [^{18}F]FB-IL-2 PET imaging," *OncoImmunology*, vol. 6, no. 1, article e1248014, 2017.

[34] V. Di Gialleonardo, A. Signore, A. W. Glaudemans, R. A. Dierckx, and E. F. De Vries, "*N*-(4-^{18}F-Fluorobenzoyl)interleukin-2 for PET of human-activated T lymphocytes," *Journal of Nuclear Medicine*, vol. 53, no. 5, pp. 679–686, 2012.

[35] S. T. G. Bruijnen, D. Chandrupatla, L. Giovanonni et al., "F8-IL10: a new potential antirheumatic drug evaluated by a PET-guided translational approach," *Molecular Pharmaceutics*, vol. 16, no. 1, pp. 273–281, 2019.

[36] D. Shi, W. Liu, S. Zhao, C. Zhang, T. Liang, and G. Hou, "TLR5 is a new reporter for triple-negative breast cancer indicated by radioimmunoimaging and fluorescent staining," *Journal of Cellular and Molecular Medicine*, vol. 23, no. 12, pp. 8305–8313, 2019.

[37] M. N. Ceylan, S. Akdas, and N. Yazihan, "The effects of zinc supplementation on C-reactive protein and inflammatory cytokines: a meta-analysis and systematical review," *Journal of Interferon & Cytokine Research*, vol. 41, no. 3, pp. 81–101, 2021.

[38] H. Ding, M. Carlton, S. Povoski et al., "Site specific discrete PEGylation of ^{124}I-labeled mCC49 Fab' fragments improves tumor microPET/CT imaging in mice," *Bioconjugate Chemistry*, vol. 24, no. 11, pp. 1945–1954, 2013.

[39] R. Zhang, "Donor-specific antibodies in kidney transplant recipients," *Clinical Journal of the American Society of Nephrology*, vol. 13, no. 1, pp. 182–192, 2018.

[40] L. Belle, K. Agle, V. Zhou et al., "Blockade of interleukin-27 signaling reduces GVHD in mice by augmenting Treg reconstitution and stabilizing Foxp3 expression," *Blood*, vol. 128, no. 16, pp. 2068–2082, 2016.

[41] J.-Y. Jung, L. L. Roberts, and C. M. Robinson, "The presence of interleukin-27 during monocyte-derived dendritic cell differentiation promotes improved antigen processing and stimulation of T cells," *Immunology*, vol. 144, no. 4, pp. 649–660, 2015.

[42] C. Petes, V. Mintsopoulos, R. L. Finnen, B. W. Banfield, and K. Gee, "The effects of CD14 and IL-27 on induction of endotoxin tolerance in human monocytes and macrophages," *The*

Journal of Biological Chemistry, vol. 293, no. 45, pp. 17631–17645, 2018.

[43] Y. H. Choi, E. J. Lim, S. W. Kim, Y. W. Moon, K. S. Park, and H.-J. An, "IL-27 enhances IL-15/IL-18-mediated activation of human natural killer cells," *Journal for Immunotherapy of Cancer*, vol. 7, no. 1, pp. 168–168, 2019.

[44] Y. Iwasaki, K. Fujio, T. Okamura, and K. Yamamoto, "Interleukin-27 in T cell immunity," *International Journal of Molecular Sciences*, vol. 16, no. 2, pp. 2851–2863, 2015.

[45] K. Holz, M. Prinz, S. M. Brendecke et al., "Differing outcome of experimental autoimmune encephalitis in macrophage/neutrophil- and T cell-specific gp130-deficient mice," *Frontiers in Immunology*, vol. 9, p. 836, 2018.

[46] S. Zhao, T. Liang, C. Zhang et al., "IL-27 Rα^+ cells promoted allorejection via enhancing STAT1/3/5 phosphorylation," *Journal of Cellular and Molecular Medicine*, vol. 24, no. 18, pp. 10756–10767, 2020.

[47] V. Calzada, M. F. García, L. M. Alonso-Martínez et al., "Fab(-nimotuzumab)-HYNIC-99mTc: antibody fragmentation for molecular imaging agents," *Anti-Cancer Agents in Medicinal Chemistry*, vol. 16, no. 9, pp. 1184–1189, 2016.

[48] A. Glaudemans, E. Bonanno, F. Galli et al., "In vivo and in vitro evidence that ^{99m}Tc-HYNIC-interleukin-2 is able to detect T lymphocytes in vulnerable atherosclerotic plaques of the carotid artery," *European Journal of Nuclear Medicine and Molecular Imaging*, vol. 41, no. 9, pp. 1710–1719, 2014.

[49] E. D. Telenga, W. van der Bij, E. F. J. de Vries et al., "^{99m}Tc-HYNIC-IL-2 scintigraphy to detect acute rejection in lung transplantation patients: a proof-of-concept study," *EJNMMI Research*, vol. 9, no. 1, p. 41, 2019.

[50] F. Galli, M. Artico, S. Taurone et al., "Radiolabeling of VEGF165 with 99mTc to evaluate VEGFR expression in tumor angiogenesis," *International Journal of Oncology*, vol. 50, no. 6, pp. 2171–2179, 2017.

[51] S. Gratz, H. J. Rennen, O. C. Boerman, W. J. Oyen, and F. H. Corstens, "Rapid imaging of experimental colitis with (99m)Tc-interleukin-8 in rabbits," *Journal of Nuclear Medicine*, vol. 42, no. 6, pp. 917–923, 2001.

[52] G. A. Sedik, R. S. A. Rizq, I. T. Ibrahim, E. S. Elzanfaly, and M. A. Motaleb, "Miniaturized chromatographic systems for radiochemical purity evaluation of ^{131}I-ferulic acid as a new candidate in nuclear medicine applications," *Applied Radiation and Isotopes*, vol. 167, article 109370, 2021.

[53] K. Matsushima, J. Yodoi, Y. Tagaya, and J. J. Oppenheim, "Down-regulation of interleukin 1 (IL 1) receptor expression by IL 1 and fate of internalized 125I-labeled IL 1 beta in a human large granular lymphocyte cell line," *The Journal of Immunology*, vol. 137, no. 10, pp. 3183–3188, 1986.

[54] J. C. Nieto, E. Cantó, C. Zamora, M. A. Ortiz, C. Juárez, and S. Vidal, "Selective loss of chemokine receptor expression on leukocytes after cell isolation," *PLoS One*, vol. 7, no. 3, article e31297, 2012.

[55] K. Ohtsubo and J. D. Marth, "Glycosylation in cellular mechanisms of health and disease," *Cell*, vol. 126, no. 5, pp. 855–867, 2006.

[56] M. G. Matera, L. Calzetta, P. Rogliani, and M. Cazzola, "Monoclonal antibodies for severe asthma: pharmacokinetic profiles," *Respiratory Medicine*, vol. 153, pp. 3–13, 2019.

[57] T. Hemmerle, C. Hess, D. Venetz, and D. Neri, "Tumor targeting properties of antibody fusion proteins based on different members of the murine tumor necrosis superfamily," *Journal of Biotechnology*, vol. 172, pp. 73–76, 2014.

[58] F. Gao, S. Zhao, and G. Hou, *Development and evaluation of a novel radiotracer 125I-rIL-27 to monitor allotransplantation rejection by specifically targeting IL-27Rα*, Research Square, 2021.